Unveiling Oxygen Vacancy Superstructures in Reduced Anatase Thin Films

Daniel Knez,[*,†] Goran Dražić,[‡] Sandeep Kumar Chaluvadi,[†] Pasquale Orgiani,[†] Stefano Fabris,[†] Giancarlo Panaccione,[†] Giorgio Rossi,[†,¶] and Regina Ciancio[*,†]

†*Istituto Officina dei Materiali-CNR, Area Science Park, S.S.14, Km 163.5, 34149 Trieste, Italy*

‡*Department of Materials Chemistry, National Institute of Chemistry, Hajdrihova 19, 1001 Ljubljana, Slovenia*

¶*Dipartimento di Fisica, Università degli Studi di Milano, Via Celoria 16, 20133 Milano, Italy*

E-mail: knez@iom.cnr.it; ciancio@iom.cnr.it

Abstract

Oxygen vacancies are known to play a crucial role in tuning the physical properties and technological applications of titanium dioxide TiO_2. Over the last decades, defects in substoichiometric TiO_2 have been commonly associated to the formation of Ti_nO_{2n-x} Magnéli phases, that are extended planar defects originating from crystallographic shear planes. By combining advanced transmission electron microscopy techniques, electron energy-loss spectroscopy and atomistic simulations, we reach new understanding of the oxygen vacancy induced structural modulations in anatase, ruling out the earlier shear-plane model. Structural modulations are instead shown to be due to the formation of oxygen vacancy superstructures that extend periodically inside the films, preserving the crystalline order of anatase. Elucidating the structure of oxygen defects in anatase is

a crucial step for improving the functionalities of such material system and to engineer devices with targeted properties.

Keywords

structure of reduced anatase thin films, oxygen vacancy superstructures, structural modulations, Magnéli phases, shear planes, scanning transmission electron microscopy

Titanium dioxide TiO_2 is among the most investigated transition metal oxides due to its optical transparency, catalytic activity and electrochemical stability,[1–3] which makes it suitable for multiple applications in optoelectronics and photo-electrochemistry. TiO_2 crystallizes in either the rutile, brookite or anatase polymorph, all of them comprised of distorted TiO_6 octahedra. Anatase, however, shows superior photocatalytic activity as compared to rutile and brookite and is thus the preferred configuration for applications.[4,5] Even though stoichiometric anatase is known to be a wide band gap semiconductor with an indirect optical band gap of 3.2 eV, its electronic properties are largely determined by the presence of excess electrons, which can be induced by intrinsic defects, dopands or photoexcitation.[5–7] It is known that oxygen vacancies (V_O) are inherently present in anatase with a typical concentration of $10^{17}\,cm^{-3}$, which act as donors in the n-type semiconductor.[8] V_O induce localized electronic states within the band gap, correlated to the formation of Ti^{3+} ions.[6,9] Creating such in-gap states by V_O is a way to expand the photocatalytic activity of the material into the visible range of light.[10,11] Furthermore, V_O play a major role in memristive devices, where highly conductive nanofilaments are attributed to formation and disruption of Magnéli phases,[12] which are also claimed to occur nanoscopically in anatase powders after thermal treatment above 800 °C[13] and to be at the origin of the storage of alkali metals in TiO_2-based battery materials.[14,15] Understanding the low energy properties of anatase is key to guide the material engineering for optimal functionalities and the intrinsic self-doping due to the oxygen vacancy concentration and site distribution is one central aspect to be clarified.

However, while V_O in TiO_2 have been extensively studied at surface and subsurface level,[9,16–23] V_O formation and structure in bulk anatase still remains elusive.[24] Recently, vacancy induced atomic displacements have been investigated by using EXAFS,[24,25] and subsurface vacancy clustering upon annealing has been reported via Scanning Tunneling Microscopy,[19] for instance. Although these experimental techniques allowed to disclose several fundamental properties of oxygen vacancies, they could not assess their arrangement inside the crystal.

In this regard, transmission electron microscopy (TEM) provides a unique opportunity to probe the structure and image defects with atomic resolution within the bulk of the material. Previous TEM studies on anatase thin films with uncorrected microscopes, suggested the formation of crystallographic shear planes along the [103]- and [101] axis extending all over the film thickness, analogous to the Magnéli (Ti_nO_{2n-x}) phases found in oxygen-deficient rutile.[26–29] Experimental limitations, however, imposed large challenges for conclusive analysis and the occurrence of Magnéli like phases in anatase has to be finally confirmed.

We provide an unprecedented nanostructural analysis of the distribution and the ordering of V_O in anatase by relying on the most recent technological advancements in electron microscopy techniques especially regarding light elements analysis, coupled with atomistic calculations. In particular, we report on the formation of oxygen vacancy arrays in reduced anatase thin films, grown by pulsed laser deposition (PLD). Indeed, due to the recent developments in thin film growth techniques and to the high structural and chemical similarities between anatase TiO_2 and (100)-oriented lanthanum aluminate $LaAlO_3$ (LAO) substrates, thin films exhibiting structural properties comparable with those characteristic of single-crystals can be made.[30,31]

By applying high resolution TEM (HRTEM), selected area electron diffraction (SAED) and aberration corrected scanning TEM (STEM), complemented by multislice simulations based on structures obtained from Molecular Dynamics (MD) simulations, we shed light on the structural modulations characteristic of anatase and determine unambiguously the atomic structure and ordering of oxygen vacancies of the planar defects. Our results are further

supported by electron energy loss spectroscopy (EELS), which enlightens local variances in the Ti^{3+}/Ti^{4+} population. In contrast to the general assumption that correlates the phase contrast of the structural modulations in conventional TEM images to the presence of Magnéli-phases, our experimental layout along with numerical simulations point instead to the stable formation of ordered distributions of V_O, forming extended periodic superstructures with variable oxygen concentration inside the anatase thin films, with no presence of crystallographic shear planes.

A representative view of the cross-sectional region of an anatase film on LAO (100) is given in Figure 1a, showing a TEM bright field (BF) micrograph (details on sample preparation and experimental parameters are found in the Supporting Information). From this image taken at the film/substrate interface and the corresponding fast Fourier transform (FFT), we see that the interface is straight and sharp and that film and substrate fully match in plane, as a consequence of the very low lattice mismatch of anatase with the LAO substrate (approximately 0.1%).[6,9,26] The film is approximately 16 nm thick and has a typical domain structure, as observed in previous works and visible in the image where a domain boundary can be discerned. Periodic phase contrast modulations are clearly identified in the whole film with a predominant [103] orientation and a slightly varying periodicity of approximately 1.4-1.8 nm. The periodic modulations yield distinct spots in the FFT adjacent to the characteristic anatase reflection and commensurate to the periodicity measured in real space.

The SAED pattern in Figure 1b was obtained from a region containing both substrate and film. All principal reflections in the present diffraction pattern can be assigned to either LAO or anatase with no trace of other phases. However, the presence of periodic structural modulations causes additional weak satellite diffraction spots adjacent to the anatase reflections. Alignment and distance of the satellite spots match the contrast modulations visible in the TEM image. Slight variations in direction and periodicity of the structures, also visible from the real-space images, explain the diffuse appearance of the satellites. A closer

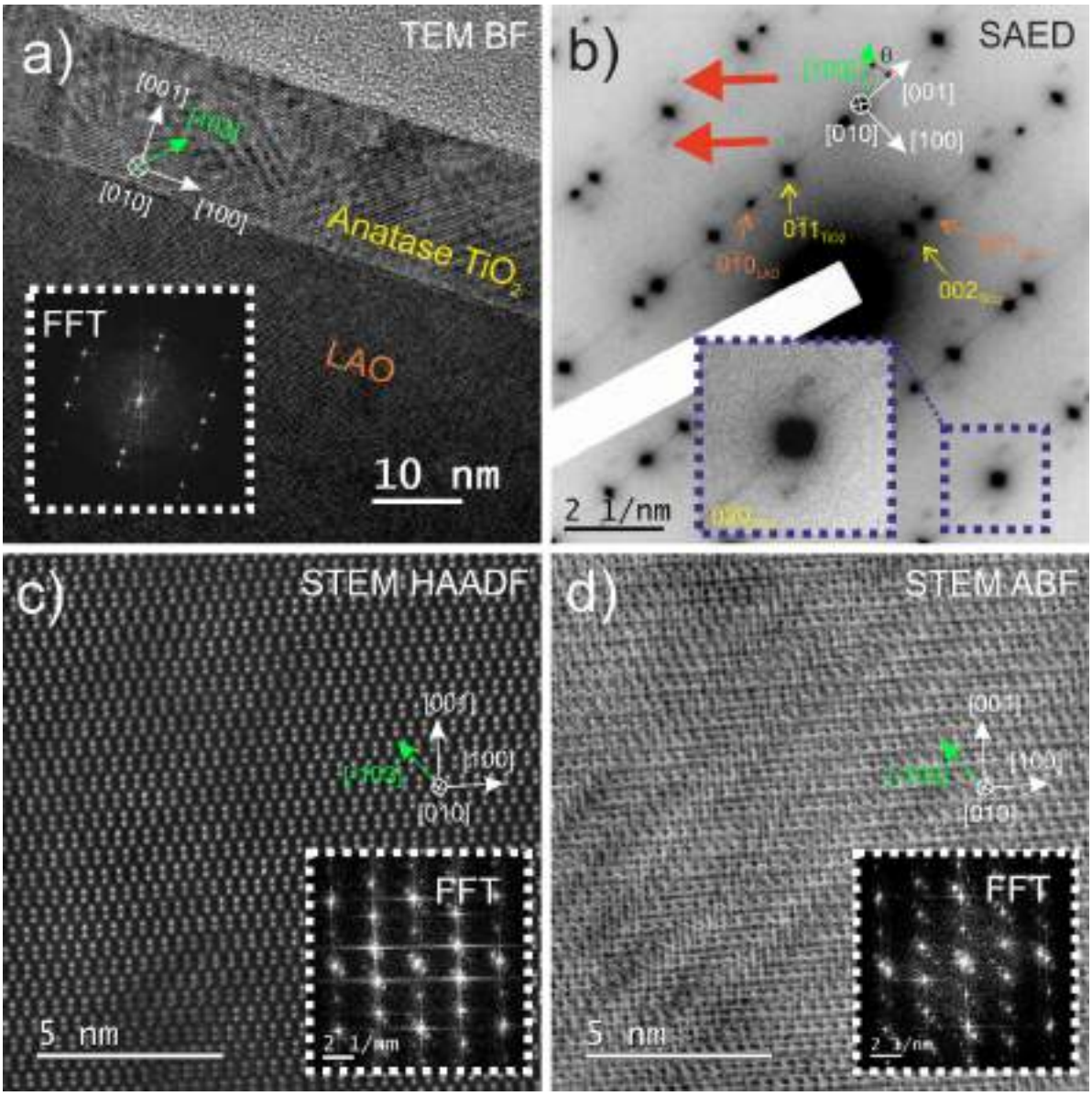

Figure 1: Cross-sectional analysis of the film/substrate area: (a) TEM BF image of the anatase film on the LAO substrate. Phase contrast clearly reveals the existence of periodic superstructures in the anatase [103] crystallographic direction. The corresponding FFT is depicted in the inset. (b) SAED pattern confirming the presence of periodic structures with the corresponding satellite spots marked by red arrows. The inset shows a magnified image of a single diffraction spot with its satellite reflections, illustrating the elongated shape of the spot in [001] direction. (c-d) Overview STEM images of the anatase region using the HAADF (c) and ABF (d) signal, both acquired simultaneously. Insets show the corresponding FFTs.

look on their shape reveals broadening along the [001] direction, which is also likely due to slight variations in direction of the arrays. A value of approximately 39 deg was measured for θ, which is the angle of the direction of the satellite spots with regard to the [001] orientation. This value matches well the expected value of 40 deg for the [103] crystallographic direction in anatase. Despite being the dominant orientation, we also identified modulations along [101] and [001] in our experiments, which is also in accordance to previous reports where contrast modulations and arrays of defects are always attributed to Ti_nO_{2n-x} Magnéli phases.[26,32] Note that the SAED intensities I have been transformed by $\frac{1}{\sqrt[3]{I}}$ for better visibility of low intensity spots.

To further elucidate the origin of the periodic contrast modulations we performed aberration-corrected STEM (see Supporting Information for details). Figure 1c shows a STEM HAADF image of a cross-sectional region within the anatase film. The HAADF signal is dominated by the Ti sublattice due to the strong dependence of high-angle electron scattering on the atomic number Z. The typical anatase dumbbell structure is clearly distinguishable in the film and recurs over the entire crossectional region with no sign of presence of secondary phases, consistently with the SAED data. The contrast modulations observed in TEM BF are also visible in HAADF, though less pronounced for the absence of phase contrast inherent to STEM HAADF imaging. As the intensity of lighter elements is better emphasized in ABF imaging, we compare the high-angle annular dark-field (HAADF) and annular bright field (ABF) signals of the same region to relate the modulations to the oxygen distribution. Figure 1d shows an ABF image acquired simultaneously with the HAADF signal from (c). Higher magnification micrographs of the same region are given in Fig. 2(a-b). Note that, opposite to HAADF, atomic columns appear dark in the ABF angular detection range. Both HAADF and ABF provide clear evidence that the periodic phase contrast variations in Figure 1 are not related to Magnéli phases, whose characteristic fingerprint is the presence of crystallographic shear planes, namely lattice discontinuities and additional lattice columns resulting from shifts of the cation positions due to the elimination of oxygen planes.[26,29,33,34]

On the contrary, the contrast modulations are characterized by blurring of atomic columns and slight atomic misalignments, while the typical anatase dumbbell structure is preserved (see the Supporting Information for a Multislice simulation based on the shear plane structure model as comparison). In particular, the ABF signal shows strong distortions of the oxygen sub-lattice, which reflect into the distribution of blurred Ti columns in the HAADF contrast. This correspondence is further highlighted in Fig. 2d where the HAADF signal from (a) and the ABF signal from (b) are combined in one image. The inset highlights a transition region between a distorted and less distorted lattice (marked by a dotted line). This finding points to a direct connection between the distortions of the O sub-lattice and the blurring of the Ti columns.

To obtain quantitative information about the distribution and arrangement of the lattice distortions we take a closer look on the spatial distribution of the HAADF signal. Figure 2c provides the result of an intensity evaluation based on the HAADF image in (a). The colours in this graph correspond to the intensity integrated over each atomic column separately[35] (see Supporting Information for details). The periodic arrays with change in intensity can be discerned in the image. Ti columns within distorted regions (blue coloured) exhibit a significant drop in intensity, compared to those outside (green-to-yellow coloured). A closer look also reveals remarkable intensity variations between the two columns of the same Ti dumbbell. Our experimental results provide evidence that the periodic contrast modulations observed in anatase by TEM are caused by the periodic arrangement of oxygen vacancies, that differently from the rutile Magnéli phases, do not yield the formation of crystallographic shear planes.

Further evidence that the structural modulations are related to the presence of V_O rich and V_O depleted regions is given by EELS analysis. EELS data shown in Figure 3 contain both edges Ti L and the O K and compare the spectrum acquired from a more distorted, V_O rich region, appearing dark in HAADF with one from a less distorted, V_O poor and

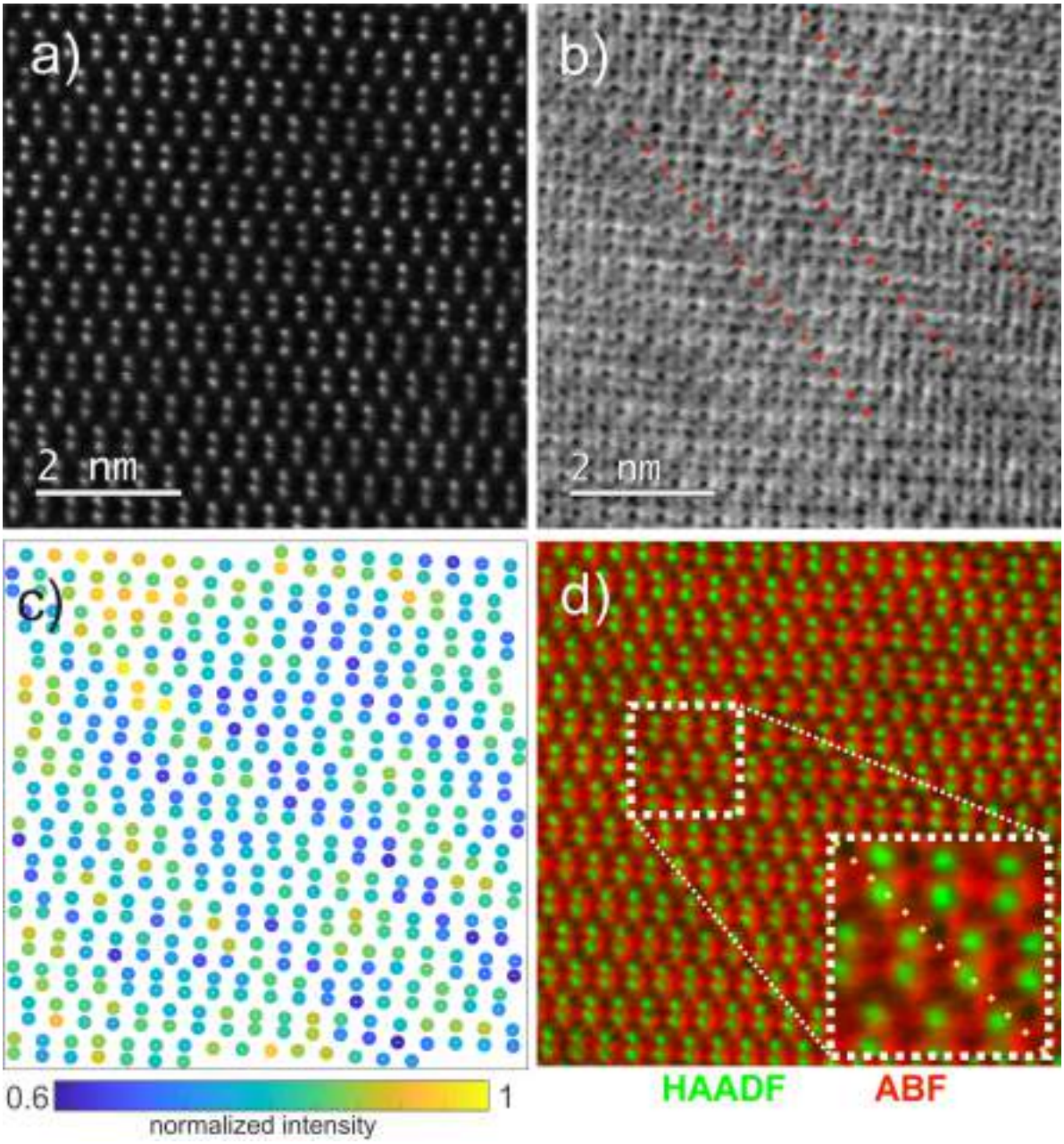

Figure 2: Experimental high resolution STEM images: (a) STEM HAADF image showing slight intensity variations within the anatase film caused by the superstructures along the in [103] direction. (b) ABF image acquired simultaneously with the HAADF signal in (a). Red lines indicate the positions of disturbed regions within the modulations. (c) Columnwise integrated intensity map generated from the HAADF image in (a). The intensity scale is normalized to the maximum integrated intensity value. The dashed red lines superimposed to the image are guide to the eyes to better identify the periodic arrays. (d) Overlay of the HAADF in (a) and ABF in (b), inset showing the transition between a V_O rich and V_O poor region; the border is indicated by a yellow dotted line.

therefore brighter area. In the latter case, the fine structure shows all characteristic anatase features,[36] while in the case of the more distorted region we see typical features of oxygen deficient anatase.[37,38] For an easier comparison of the important features we performed multiple Gaussian fitting and refer to the fit energy positions and amplitudes in the following. The presence of lower oxidation states is especially visible in the O K edge by the change in intensity ratio and splitting between t_{2g} and e_g.[39] The intensity ratio t_{2g}/e_g changes from 1.15 in the V_O depleted region to 0.93 in the V_O rich region, while the energy splitting between the two peaks changes from 3 eV to 2.6 eV. The slightly decreased t_{2g}-e_g crystal field splitting indicates a change in Ti-O bonding and hints, together with the more distinct e_g splitting in Ti L_3 (the intensity ratio of the e_g main peak to its sub-peak changes from 1.8 to 1.4), towards a decrease in crystal symmetry within the dark regions,[9,36,37,40,41] which is also in accordance to our HAADF and ABF results. Quantitative EELS based on the Ti L and O K edge intensities furthermore yields an estimate for the reduction rate of (16 $\pm$ 9) %, relative to stoichiometric TiO_2 (see the Supporting Information for details).

V_O are known to introduce significant local lattice distortions that, to first order, are driven by electrostatics: The O atoms nearest neighbour to the O vacancy displace radially towards it, while adjacent Ti atoms relax outwards.[23,42] The occurrence of these lattice distortions determine the reduction of the HAADF intensity in the corresponding Ti columns.[25] Further reduction in intensity is likely caused directly by the reduced amount of oxygen atoms within Ti columns, also contributing to the Ti dominated HAADF signal. The expected atomic displacements induced by the presence of a single vacancy are illustrated in Figure 4.

To further support the above experimental evidences that the periodic distortions measured by HAADF are indeed caused by the presence of oxygen vacancies, we compare the experimental results with multislice calculations based on geometric configurations as obtained from atomistic simulations. To this end, we randomly generate an oxygen deficient

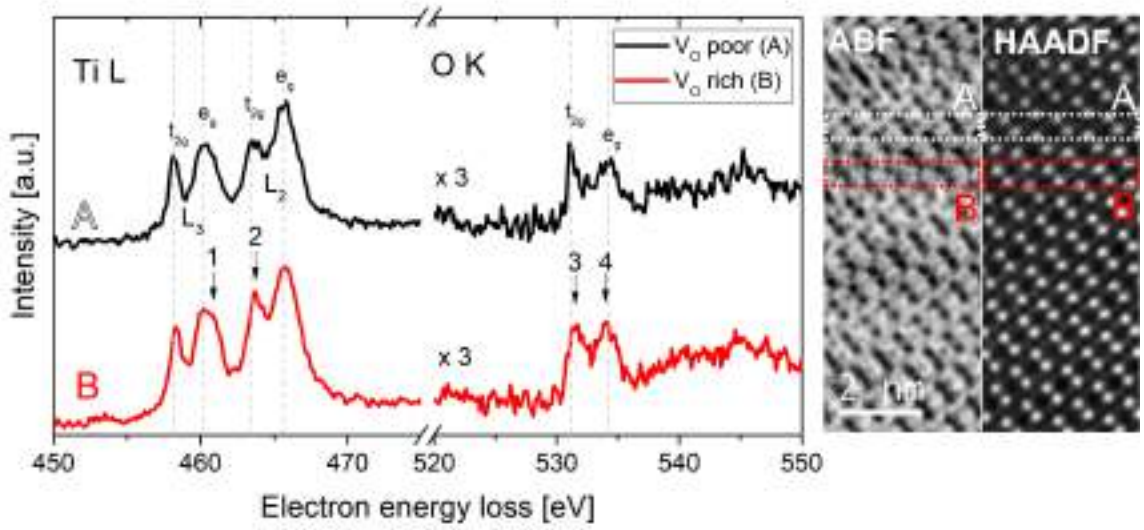

Figure 3: EELS analysis comparing the Ti L and O K fine structure of a less distorted (V_O poor) region in the film with a region exhibiting visible lattice distortions (V_O rich). The corresponding regions of spectra acquisition are indicated in the HAADF and ADF image in the inset, both showing the same sample region; spectra are shown after background subtraction and zero-loss deconvolution. The O K energy range is scaled by a factor of 3 to increase visibility. Features indicating the presence of lower valence states and coordination changes are indicated by arrows in spectrum B.

anatase geometry consistent with both our experimental findings and the DFT calculated interactions among oxygen vacancies in anatase.[42] Lattice distortions due to vacancies act as an attractive force between vacancies, while, local charge accumulation imposes a barrier for vacancy clustering.[19] The resulting energetically favorable arrangements of two oxygen vacancies are shown in Figure 4b and referred to as I and II. It is important to note that the mutual interaction between the vacancies was found to be predominant along the direction of the base vectors a or b of the anatase unit cell (corresponding to the [100] or [010] direction, depending on the vacancy position), while other configurations can be regarded as uncorrelated.

To account for the periodic vacancy arrangement on a larger scale, as probed by our experiments, the vacancies were created randomly according to a sine square probability distribution with a periodicity of 1.5 nm, along the [103] and [013] crystallographic planes, until

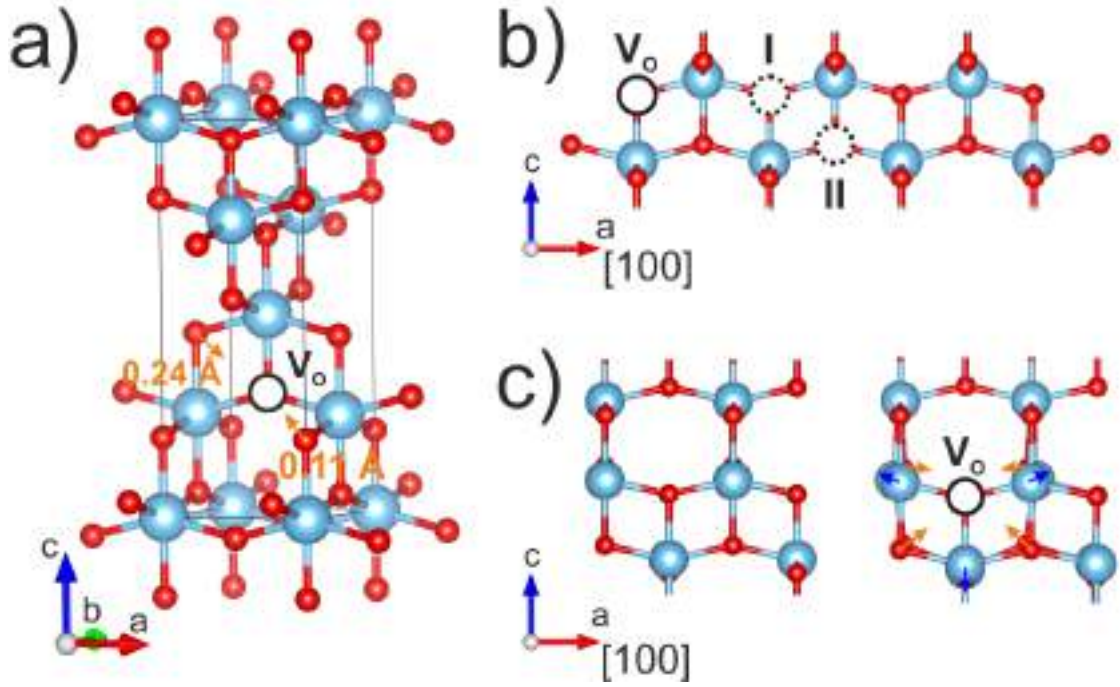

Figure 4: Lattice distortions induced by a oxygen vacancy: (a) Tetragonal unit cell of anatase with one oxygen vacancy induced (O atoms in red, and Ti atoms in cyan). Distances correspond to the V_O induced displacement of O atoms adjacent to a vacancy with regard to equilibrium distances, as predicted by ReaxFF. (b) The two energetically favorable configurations of two vacancies along the [100] or [010] atomic stripes according to DFT calculations.[42] Both I and II are energetically equivalent. (c) Visualisation of lattice distortions induced by the presence of a single oxygen vacancy (V_O) after energy minimization using ReaxFF. Orange and blue arrows represent the direction of vacancy induced displacement for O and Ti atoms, respectively.

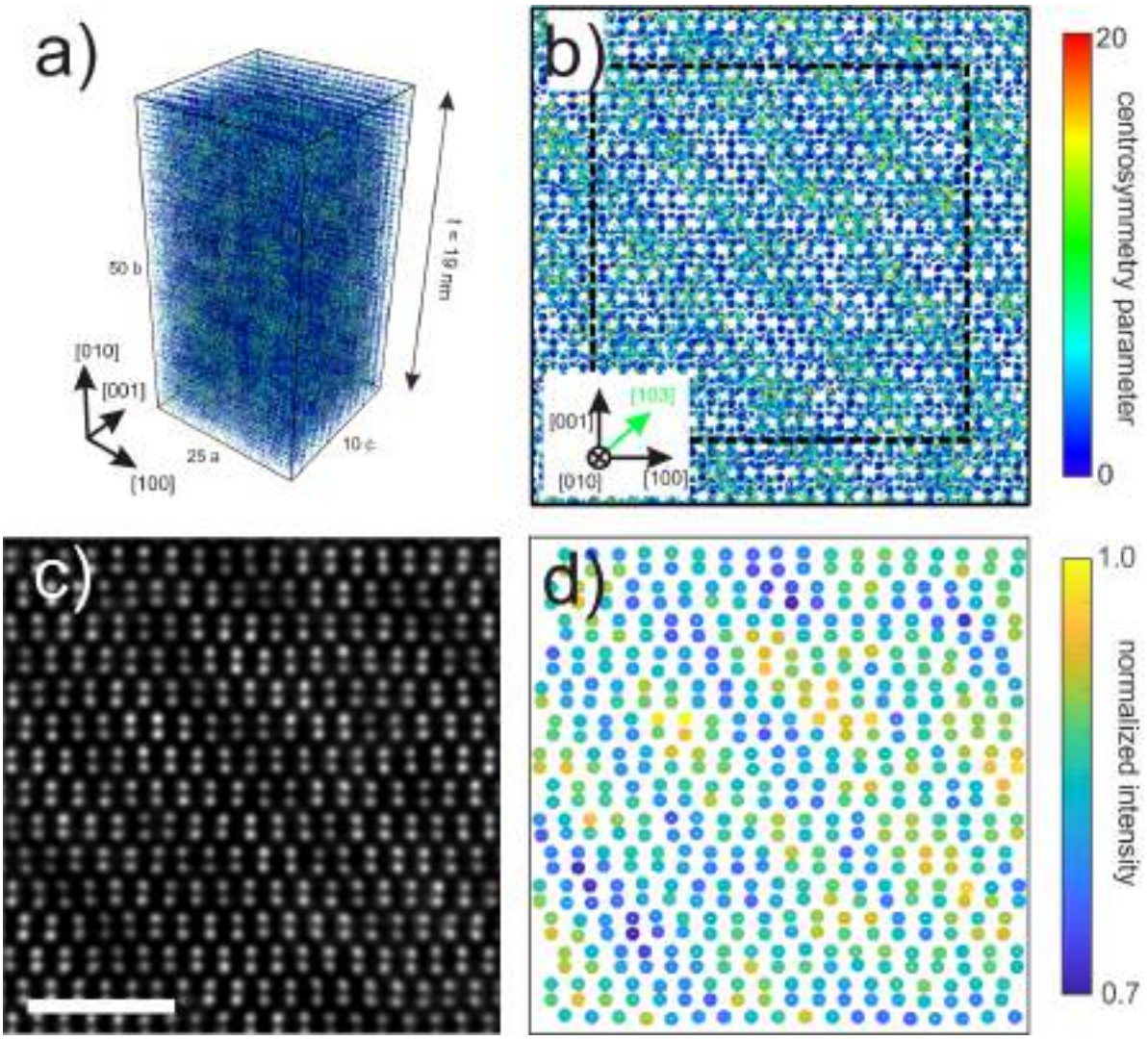

Figure 5: Atomistic simulation results: (a) Oxygen deficient (15 %) anatase supercell (25x50x10 unit cells), generated randomly according to the vacancy interaction rules based on DFT;[42] colors correspond to the centrosymmetry parameter, as a measure of the local lattice disorder[43] to guide the eye; colorbar is same as in (b). (b) View along the [010] orientation of the equilibrated geometry, exhibiting vacancy arrays. The black rectangle highlights the scan range used for image simulations. (c) Multislice simulation of HAADF contrast based on the geometry (a-b). The simulated image consist of 256x256 sampling points and is the result after 20 TDS runs. scale bar is 2 nm (d) Columnwise integrated intensity of the image in (d), normalized to the maximum value.

the desired target vacancy concentration is reached over the whole crystal. Both vacancy arrangements I and II were considered with same probability as they were calculated to be equal in energy. Here, we present the results for an overall oxygen deficiency of 15%, a value that was found to fit well the HAADF contrast in the experimental data, as well as to the O concentration estimated from the EELS data. The resulting anatase supercell has a size of 25x50x10 unit cells. After generation the geometry is energy minimized and thermalized at 300 K in an MD run (see Supporting Information). The energy minimized structure is depicted in Figure 5a and b. Subsequently, 20 configurations were extracted at different MD time steps, to sample the thermal displacements within the frozen lattice approximation during the multislice simulation. For each MD configuration a separate calculation was performed and the resulting image represents the pixel-wise averaged intensities of the 20 single images.

The central region of the supercell, $71\,\text{Å} \times 71\,\text{Å}$ in size, was selected as scan window for the calculations, while the thickness was 190 Å (corresponding to the 50 unit cells of the super cell). The selected region is shown in (b), marked by a black rectangle. The resulting HAADF image is depicted in (c). It consists of 256x256 sampling points and a slice thickness of approximately 1 Å was chosen. The periodic contrast variations of the simulated image are in a very good agreement with the experiment. This close correspondence further confirms the TEM experimental findings: periodic modulations in anatase are associated with oxygen vacancy superstructures occurring periodically inside the film. The blurring effect attributed to local atomic displacements caused by oxygen vacancies is consistent with the electrostatic relaxation behaviour of such point defects in anatase, as predicted theoretically [23,42] and also observed experimentally. [24,25] The V_O induced lattice distortions in anatase are likely compensated by the formation of V_O depleted regions and determine a long-range periodic array of modulated V_O concentration. As a consequence, the concentration modulations allow to balance expansive and compressive regions and thereby stabilize the structure, with [103] and [013] being the energetically favourable orientation, as previously reported. [17,26,44,45]

These results are also in good agreement to previous calculations for rutile, where planar V_O arrangements were discussed to form without strong atomic restructuring,[46] as well as with the general picture of defect ordering in transition metal oxides.[47]

In conclusion, we investigated the intrinsic structure of defect arrays in anatase TiO_2 thin films on LAO substrates. Aberration-corrected STEM HAADF and ABF analyses, complemented by phase contrast imaging and SAED unveiled the presence of structural modulations inside the film, that consist of periodic arrays of oxygen vacancy superstructures forming a long-range ordered structure that does not break the anatase continuity. Site selective EELS analysis demonstrated that the structural modulations are associated with alternating oxygen content regions which reflect into a Ti^{3+}/Ti^{4+} mixed population.

Our experimental findings along with extensive atomistic and multislice simulations lead to validate a new model for the defect structures in anatase that excludes the typical shear-plane structures, like the Ti_nO_{2n-x} Magnéli phases, which are commonly claimed to occur in titanium dioxide. Our study provides a conclusive picture on the intrinsic structural assessment of oxygen vacancy superstructures in reduced TiO_2 anatase thin films and enlightens the great power of combining advanced TEM and simulation techniques to address secondary structures in complex materials.

Supporting Information Available

This material is available free of charge via the internet at http://pubs.acs.org.

In the Supporting Information we provide details on the TEM experiments and sample preparation, as well as parameters for MD and multislice calculations. It furthermore contains details on the PLD growth conditions and pre-characterisation of the films based on XRR, XAS, XRD and XPS measurements, performed at the NFFA facility integrating the APE beamlines of IOM-CNR at Elettra in Trieste. We also give additional views on the oxygen deficient supercell used for the simulations in Figure 4, multislice simulations of the

shear plane model in comparison, a complementary ABF simulation, details on EELS quantification, and an analysis of the atomic displacements from the experimental and simulated HAADF images.

Author contributions

R.C. conceived the experiment. D.K., G.D. and R.C. performed the TEM experiments. D.K. and G.D. performed the TEM/EELS experiments by aberration corrected microscope. D.K. carried out the theoretical calculations. S.K.C. and P.O. grew the films and performed structural characterization by x-ray diffraction. S.F. contributed to the theoretical analysis. P.O. performed synchrotron radiation experiments and analyzed data. G.P. and G.R. contributed to the discussion of results and to reviewing drafts. D.K. and R.C. wrote the paper with the contribution from all the authors.

Acknowledgement

This work has been performed in the framework of the Nanoscience Foundry and Fine Analysis (NFFA-MIUR Italy Progetti Internazionali) facility. We are grateful to E. Cociancich and P. Rajak for the assistance in TEM specimen preparation and J. Kraxner for proofreading. G.D. acknowledges the financial support from the Slovenian Research Agency (P2-0393).

References

(1) Kavan, L.; Grätzel, M.; Gilbert, S. E.; Klemenz, C.; Scheel, H. J. Electrochemical and Photoelectrochemical Investigation of Single-Crystal Anatase. *Journal of the American Chemical Society* **1996**, *118*, 6716–6723.

(2) Li, Y.; Peng, Y.-K.; Hu, L.; Zheng, J.; Prabhakaran, D.; Wu, S.; Puchtler, T. J.; Li, M.; Wong, K.-Y.; Taylor, R. A.; Tsang, S. C. E. Photocatalytic water splitting by N-TiO2

on MgO (111) with exceptional quantum efficiencies at elevated temperatures. *Nature communications* **2019**, *10*, 4421.

(3) Rahimi, N.; Pax, R. A.; Gray, E. M. Review of functional titanium oxides. I: TiO2 and its modifications. *Progress in Solid State Chemistry* **2016**, *44*, 86–105.

(4) Arbiol, J.; Cerdà, J.; Dezanneau, G.; Cirera, A.; Peiró, F.; Cornet, A.; Morante, J. R. Effects of Nb doping on the TiO2 anatase-to-rutile phase transition. *Journal of Applied Physics* **2002**, *92*, 853–861.

(5) Reyes-Coronado, D.; Rodríguez-Gattorno, G.; Espinosa-Pesqueira, M. E.; Cab, C.; de Coss, R.; Oskam, G. Phase-pure TiO(2) nanoparticles: anatase, brookite and rutile. *Nanotechnology* **2008**, *19*, 145605.

(6) Gobaut, B. et al. Role of Oxygen Deposition Pressure in the Formation of Ti Defect States in Ti_2 (001) Anatase Thin Films. *ACS applied materials & interfaces* **2017**, *9*, 23099–23106.

(7) Chiodo, L.; García-Lastra, J. M.; Iacomino, A.; Ossicini, S.; Zhao, J.; Petek, H.; Rubio, A. Self-energy and excitonic effects in the electronic and optical properties of TiO2 crystalline phases. *Physical Review B* **2010**, *82*, 045207.

(8) Moser, S.; Moreschini, L.; Jaćimović, J.; Barišić, O. S.; Berger, H.; Magrez, A.; Chang, Y. J.; Kim, K. S.; Bostwick, A.; Rotenberg, E.; Forró, L.; Grioni, M. Tunable polaronic conduction in anatase TiO2. *Physical review letters* **2013**, *110*, 196403.

(9) Bigi, C. et al. Distinct behavior of localized and delocalized carriers in anatase Ti_2 (001) during reaction with O_2. *Physical Review Materials* **2020**, *4*, 025801.

(10) Zhou, Y.; Chen, C.; Wang, N.; Li, Y.; Ding, H. Stable Ti 3+ Self-Doped Anatase-Rutile Mixed TiO 2 with Enhanced Visible Light Utilization and Durability. *Journal of Physical Chemistry C* **2016**, *120*, 6116–6124.

(11) Orgiani, P.; Perucchi, A.; Knez, D.; Ciancio, R.; Bigi, C.; Chaluvadi, S. K.; Fujii, J.; Vobornik, I.; Panaccione, G.; Rossi, G.; Lupi, S.; Di Pietro, P. Tuning the Optical Absorption of Anatase Thin Films Across the Visible-To-Near-Infrared Spectral Region. *Physical Review Applied* **2020**, *13*, 044011.

(12) Kwon, D.-H.; Kim, K. M.; Jang, J. H.; Jeon, J. M.; Lee, M. H.; Kim, G. H.; Li, X.-S.; Park, G.-S.; Lee, B.; Han, S.; Kim, M.; Hwang, C. S. Atomic structure of conducting nanofilaments in TiO2 resistive switching memory. *Nature nanotechnology* **2010**, *5*, 148–153.

(13) Domaschke, M.; Zhou, X.; Wergen, L.; Romeis, S.; Miehlich, M. E.; Meyer, K.; Peukert, W.; Schmuki, P. Magnéli-Phases in Anatase Strongly Promote Cocatalyst-Free Photocatalytic Hydrogen Evolution. *ACS Catalysis* **2019**, *9*, 3627–3632.

(14) Chen, J.; Ding, Z.; Wang, C.; Hou, H.; Zhang, Y.; Wang, C.; Zou, G.; Ji, X. Black Anatase Titania with Ultrafast Sodium-Storage Performances Stimulated by Oxygen Vacancies. *ACS applied materials & interfaces* **2016**, *8*, 9142–9151.

(15) Hao, Z.; Chen, Q.; Dai, W.; Ren, Y.; Zhou, Y.; Yang, J.; Xie, S.; Shen, Y.; Wu, J.; Chen, W.; Xu, G. Q. Oxygen–Deficient Blue TiO 2 for Ultrastable and Fast Lithium Storage. *Advanced Energy Materials* **2020**, 1903107.

(16) Schaub, R.; Wahlström, E.; Rønnau, A.; Lagsgaard, E.; Stensgaard, I.; Besenbacher, F. Oxygen-mediated diffusion of oxygen vacancies on the TiO2(110) surface. *Science (New York, N.Y.)* **2003**, *299*, 377–379.

(17) Oropeza, F. E.; Zhang, K. H. L.; Regoutz, A.; Lazarov, V. K.; Wermeille, D.; Poll, C. G.; Egdell, R. G. Growth of Epitaxial Anatase Nano Islands on SrTiO 3 (001) by Dip Coating. *Crystal Growth & Design* **2013**, *13*, 1438–1444.

(18) Setvín, M.; Aschauer, U.; Scheiber, P.; Li, Y.-F.; Hou, W.; Schmid, M.; Selloni, A.;

Diebold, U. Reaction of O2 with subsurface oxygen vacancies on TiO2 anatase (101). *Science (New York, N.Y.)* **2013**, *341*, 988–991.

(19) Setvin, M.; Schmid, M.; Diebold, U. Aggregation and electronically induced migration of oxygen vacancies in TiO2 anatase. *Physical Review B* **2015**, *91*, 195403.

(20) Zhao, X.; Selcuk, S.; Selloni, A. Formation and stability of reduced TiOx layers on anatase TiO2(101) : Identification of a novel Ti2O3 phase. *Physical Review Materials* **2018**, *2*, 015801.

(21) Yin, W.-J.; Wen, B.; Zhou, C.; Selloni, A.; Liu, L.-M. Excess electrons in reduced rutile and anatase TiO 2. *Surface Science Reports* **2018**, *73*, 58–82.

(22) Selcuk, S.; Zhao, X.; Selloni, A. Structural evolution of titanium dioxide during reduction in high-pressure hydrogen. *Nature materials* **2018**, *17*, 923–928.

(23) Cheng, H.; Selloni, A. Energetics and diffusion of intrinsic surface and subsurface defects on anatase TiO2(101). *The Journal of chemical physics* **2009**, *131*, 054703.

(24) Leedahl, B.; de Boer, T.; Yuan, X.; Moewes, A. Oxygen Vacancy Induced Structural Distortions in Black Titania: A Unique Approach using Soft X-ray EXAFS at the O-K Edge. *Chemistry (Weinheim an der Bergstrasse, Germany)* **2019**, *25*, 3272–3278.

(25) Yang, Y.; Yin, L.-C.; Gong, Y.; Niu, P.; Wang, J.-Q.; Gu, L.; Chen, X.; Liu, G.; Wang, L.; Cheng, H.-M. An Unusual Strong Visible-Light Absorption Band in Red Anatase TiO2 Photocatalyst Induced by Atomic Hydrogen-Occupied Oxygen Vacancies. *Advanced materials (Deerfield Beach, Fla.)* **2018**, *30*, 1704479.

(26) Ciancio, R.; Carlino, E.; Rossi, G.; Aruta, C.; Di Scotti Uccio, U.; Vittadini, A.; Selloni, A. Magnéli-like phases in epitaxial anatase TiO 2 thin films. *Physical Review B* **2012**, *86*, 651.

(27) Chambers, S.; Wang, C.; Thevuthasan, S.; Droubay, T.; McCready, D.; Lea, A.; Shutthanandan, V.; Windisch Jr, C. Epitaxial growth and properties of MBE-grown ferromagnetic Co-doped TiO2 anatase films on SrTiO3(001) and LaAlO3(001). *Thin Solid Films* **2002**, *418*, 197–210.

(28) Ciancio, R.; Vittadini, A.; Selloni, A.; Arpaia, R.; Aruta, C.; Miletto Granozio, F.; Di Scotti Uccio, U.; Rossi, G.; Carlino, E. Evolution of nanostructures of anatase TiO2 thin films grown on (001) LaAlO3. *Journal of Nanoparticle Research* **2013**, *15*, 943.

(29) Wood, G. J.; Bursill, L. A. The Formation Energy of Crystallographic Shear Planes in TiFormulaOFormula. *Proceedings of the Royal Society A: Mathematical, Physical and Engineering Sciences* **1981**, *375*, 105–125.

(30) Schlom, D. G.; Chen, L.-Q.; Pan, X.; Schmehl, A.; Zurbuchen, M. A. A Thin Film Approach to Engineering Functionality into Oxides. *Journal of the American Ceramic Society* **2008**, *91*, 2429–2454.

(31) Chambers, S. A. Epitaxial growth and properties of doped transition metal and complex oxide films. *Advanced materials (Deerfield Beach, Fla.)* **2010**, *22*, 219–248.

(32) Ciancio, R.; Carlino, E.; Aruta, C.; Maccariello, D.; Granozio, F. M.; Di Scotti Uccio, U. Nanostructure of buried interface layers in TiO_2 anatase thin films grown on $LaAlO_3$ and $SrTiO_3$ substrates. *Nanoscale* **2012**, *4*, 91–94.

(33) van Landuyt, J. Shear Structures and Crystallographic Shear Propagation. *Le Journal de Physique Colloques* **1974**, *35*, 53–63.

(34) Bursill, L. A.; Wood, G. J. Electron-optical imaging of Ti 6 O 11 at 1·6 Å point-to-point resolution. *Philosophical Magazine A* **1978**, *38*, 673–689.

(35) Jones, L.; MacArthur, K. E.; Fauske, V. T.; van Helvoort, Antonius T J,; Nellist, P. D.

Rapid estimation of catalyst nanoparticle morphology and atomic-coordination by high-resolution Z-contrast electron microscopy. *Nano letters* **2014**, *14*, 6336–6341.

(36) Brydson, R.; Sauer, H.; Engel, W.; Thomass, J. M.; Zeitler, E.; Kosugi, N.; Kuroda, H. Electron energy loss and X-ray absorption spectroscopy of rutile and anatase: a test of structural sensitivity. *Journal of Physics C: Solid State Physics* **1989**, *1*, 797–812.

(37) Lusvardi, V. S.; Barteau, M. A.; Chen, J. G.; Eng, J.; Frühberger, B.; Teplyakov, A. An NEXAFS investigation of the reduction and reoxidation of TiO2(001). *Surface Science* **1998**, *397*, 237–250.

(38) Stoyanov, E.; Langenhorst, F.; Steinle-Neumann, G. The effect of valence state and site geometry on Ti L3,2 and O K electron energy-loss spectra of TixOy phases. *American Mineralogist* **2007**, *92*, 577–586.

(39) Brydson, R.; Sauer, H.; Engel, W.; Hofer, F. Electron energy-loss near-edge structures at the oxygen K edges of titanium(IV) oxygen compounds. *Journal of Physics: Condensed Matter* **1992**, *4*, 3429–3437.

(40) Bertoni, G.; Beyers, E.; Verbeeck, J.; Mertens, M.; Cool, P.; Vansant, E. F.; van Tendeloo, G. Quantification of crystalline and amorphous content in porous samples from electron energy loss spectroscopy. *Ultramicroscopy* **2006**, *106*, 630–635.

(41) Krüger, P. Multichannel multiple scattering calculation of L2,3 -edge spectra of TiO2 and SrTiO3 : Importance of multiplet coupling and band structure. *Physical Review B* **2010**, *81*, 140.

(42) Paris, A.; Taioli, S. Multiscale Investigation of Oxygen Vacancies in TiO 2 Anatase and Their Role in Memristor's Behavior. *The Journal of Physical Chemistry C* **2016**, *120*, 22045–22053.

(43) Kelchner, C. L.; Plimpton, S. J.; Hamilton, J. C. Dislocation nucleation and defect structure during surface indentation. *Physical Review B* **1998**, *58*, 11085–11088.

(44) Banfield, J. F.; Veblen, D. R. Conversion of perovskite to anatase and TiO2 (B): A TEM study and the use of fundamental building blocks for understanding relationships among the TiO2 minerals. *American Mineralogist* **1992**, *77*, 545–557.

(45) Banfield, J. F.; Veblen, D. R.; Smith, D. J. The identification of naturally occurring TiO2 (B) by structure determination using high-resolution electron microscopy, image simulation, and distance-least-squares refinement. *American Mineralogist* **1991**, *76*, 343–353.

(46) Heckel, W.; Wehlau, M.; Maisel, S. B.; Frauenheim, T.; Knaup, J. M.; Müller, S. How the aggregation of oxygen vacancies in rutile-based $TiO_{2-\delta}$ phases causes memristive behavior. *Physical Review B* **2015**, *92*, 214104.

(47) Stoneham, A. M.; Durham, P. J. The ordering of crystallographic shear planes: Theory of regular arrays. *Journal of Physics and Chemistry of Solids* **1973**, *34*, 2127–2135.

Graphical TOC Entry